Electronic Supplementary Material (ESI) for Journal of Materials Chemistry C.
This journal is © The Royal Society of Chemistry 2024

Electronic Supplementary Information

Lightweight porous shear stiffening composite foam with excellent mechanical-thermal coupling protection performance

Tingting Xuan,[a] Sheng Wang,*[a] Shuai Liu,[a] Wenhui Wang,[a] Zimu Li,[a] Yuan Hu[b] and Xinglong Gong*[ab]

[a] *CAS Key Laboratory of Mechanical Behavior and Design of Materials, Department of Modern Mechanics, University of Science and Technology of China, Hefei, Anhui 230027, PR China*
[b] *State Key Laboratory of Fire Science, University of Science and Technology of China, 96 Jinzhai Road, Hefei, Anhui, 230026, PR China*

Corresponding author: Tel: 86-551-63601702; Fax: 86-551-63600419.
E-mail: gongxl@ustc.edu.cn (X. L. Gong)
wsh160@ustc.edu.cn (S. Wang)

Experimental section

Materials

Hydroxyl silicone oil, boric acid, n-octanoic acid, benzoyl peroxide (BPO), dicumyl peroxide (DCP) and paraffin wax (PW, the melting point was 54 °C~56 °C) were all purchased from Sinopharm Chemical Reagent Co., Ltd, China. Ethylene vinyl acetate copolymer (EVA) was provided by Yuancheng Plastic Raw Material Co., Ltd, China. Azodicarbonmide (AC) was obtained from Duoyi Chemical Technology Co., Ltd, China. Methyl vinyl silicone rubber (VMQ) was supplied by by Kaixuan Plastic Technology Co., Ltd, China. All the chemical reagents were used as received without further purification.

Synthesis of shear stiffening gel (SSG)

First, hydroxy silicone oil and boric acid were mixed evenly with a mass ratio of 30:1 and heated at 180 °C for 2 hours. Subsequently, n-octanoic acid was added and heated for 30 min. Finally, the compound was cooled to room temperature to obtain SSG.

Preparation of SSE-EVA foam (SEF)

SSG, VMQ and the vulcanizing BPO were firstly mixed to obtain SSE precursor by using a double-roll mill. Next, EVA with different mass ratios, DCP (3% of the mass fraction of EVA) and varying amounts of AC were added to obtain a uniform mixture. The obtained mixture was then vulcanized to obtain SEF. Notably, the foams with different mass fraction of SSE precursor and EVA were named S_xE_yF. For instance, the composite was named S_3E_1F when the mass ratio of SSE precursor to EVA was 3:1.

Preparation of SEFP

SEFP was prepared through impregnation method. Firstly, solid PW was melted at 65 °C. Then, SEF was evenly immersed to ensure the total absorption of PW solution. SEFP was finally obtained after further cooling.

Characterization

The morphology of composites was characterized by scanning electron microscopes (SEM EV018, Carl Zeiss, UK). The porous structure of SEF was analyzed by an X-ray CT device (Nordson Dage Quadra 7). FTIR spectra was collected by Fourier Transform infrared spectra Microscope (Nicolet iN 10, Thermo Scientifc, USA) in ATR mode over a range of 4000-520 cm^{-1}.

The uniaxial compression test was performed using a universal electronic material testing machine (MTS, Criterion Model 43, MTS Co., Ltd, China). The impact resistance was measured using a drop hammer impact device (ZCJ1302- A, MTS, USA). The weight of the hammer was 550 g and the sample size was 20 mm × 20 mm × 5 mm. The morphological destructions of SEFs were recorded by a high-speed video camera (Phantom v2512, Vision Research, USA).

The thermal conductivities of SEFs were tested by a transient plate heat source method (Hot Disk TPS 2500 S). Thermocouple (CEM DT-8891E, China) was used to monitor the temperature of SEF, and infrared images were recorded by an infrared camera (TESTO 865). During the test, the dimensions of SEFs were 20 mm × 20 mm × 5 mm.

The calculation principle for the energy loss and energy loss coefficient of SEF:

During the compression test, SEF was compressed from its initial height (h_1) to a predetermined height (h_2). Due to the viscoelastic property of SEF, a hysteresis loop emerged during unloading (indicated by the yellow area in Fig. S4a), which represented the energy loss (ΔE) of SEF during a compression cycle.[1,2] Thus, ΔE of SEF could be formulated as:

$$\Delta E = E_i - E_r = \int F_i(h)dh - \int F_r(h)dh \tag{1}$$

where E_i was the energy absorbed during loading, E_r was the energy released during unloading. $F_i(h)$ and $F_r(h)$ represented the responses of the compressive stress with respect to the compressive displacement during loading and unloading, respectively. Consequently, the energy loss coefficient of SEF could be described as:

$$\Delta e = \frac{\Delta E}{E_{max}} \tag{2}$$

Which represented the degree of the energy loss.

Finite element simulation of the thermal transfer behavior

COMSOL Multiphysics software was used to simulate the temperature distribution. The isotropic thermal conductivity, density and constant-pressure heat capacity of SEF were set as 0.121 W/(m·K), 383.3 kg/m^3 and 1753.7 J/(kg·K), and the corresponding values of PW were 0.274 W/(m·K), 880 kg/m^3 and 7005.3 J/(kg·K), respectively. The grid was divided into hexahedral units with a total number of 1000000, and the number of vertices was 1030301. The bottom of the sample was set to be a heat source with a constant temperature of 423.15 K, and the isotropic thermal conductivity, density and constant-pressure heat capacity were 45 W/(m·K), 7850 kg/m^3 and 460 J/(kg·K), respectively. The external temperature was maintained at 298.15 K, which was consistent with the room temperature, and the convective heat transfer coefficient of the sample with the external space was 5 W/(m^2·K).

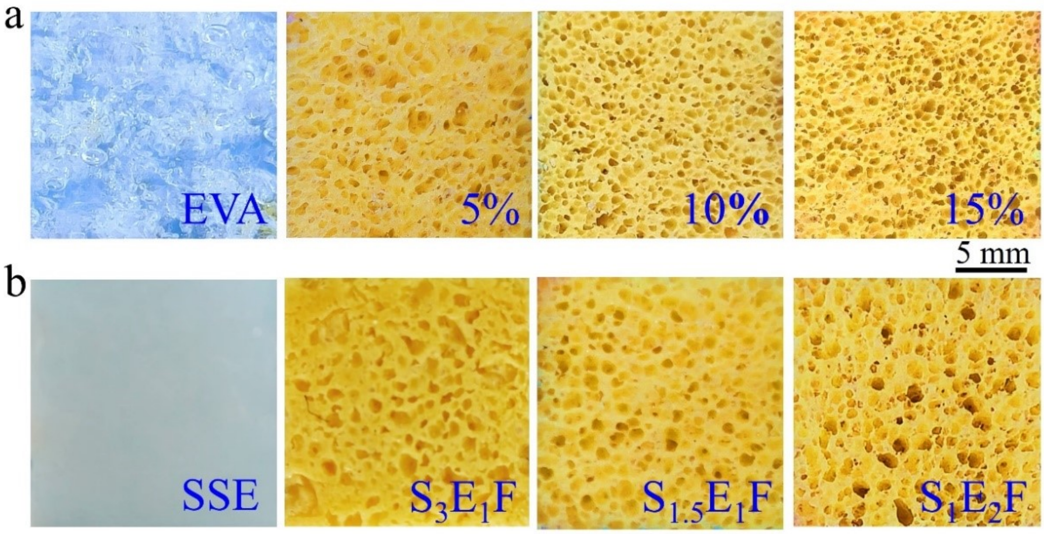

Fig. S1 (a) Morphology diagrams of EVA and S_1E_1F with different AC content. (b) Digital images of SEF with different mass fractions of SSE and EVA.

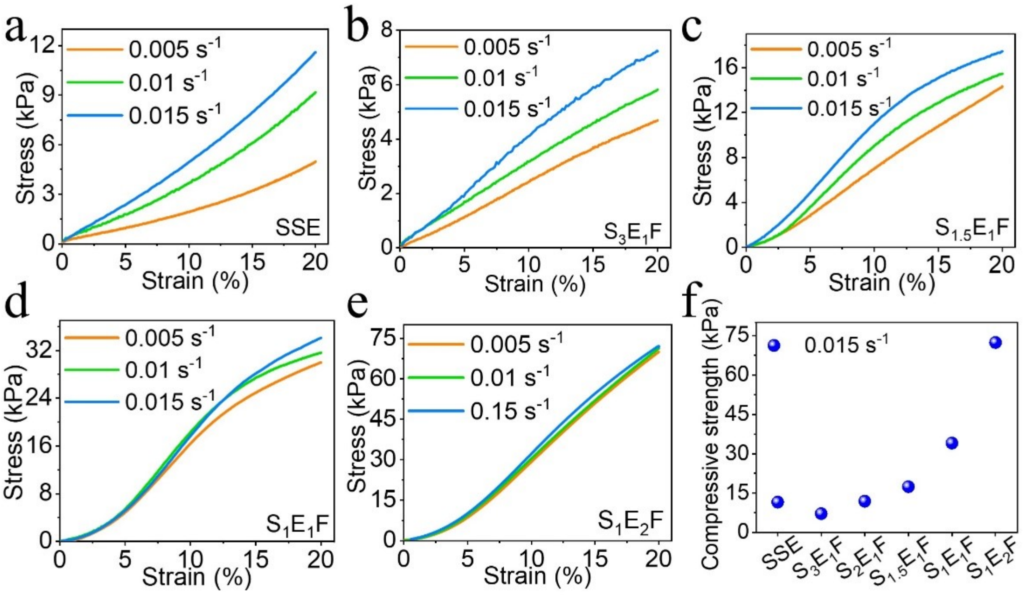

Fig. S2 Mechanical behavior of S_xE_yF. Stress-strain curves of (a) SSE, (b) S_3E_1F, (c) $S_{1.5}E_1F$, (d) S_1E_1F and (e) S_1E_2F at different compressive strain rates. (f) Compressive strength of S_xE_yF at 0.015 s^{-1}.

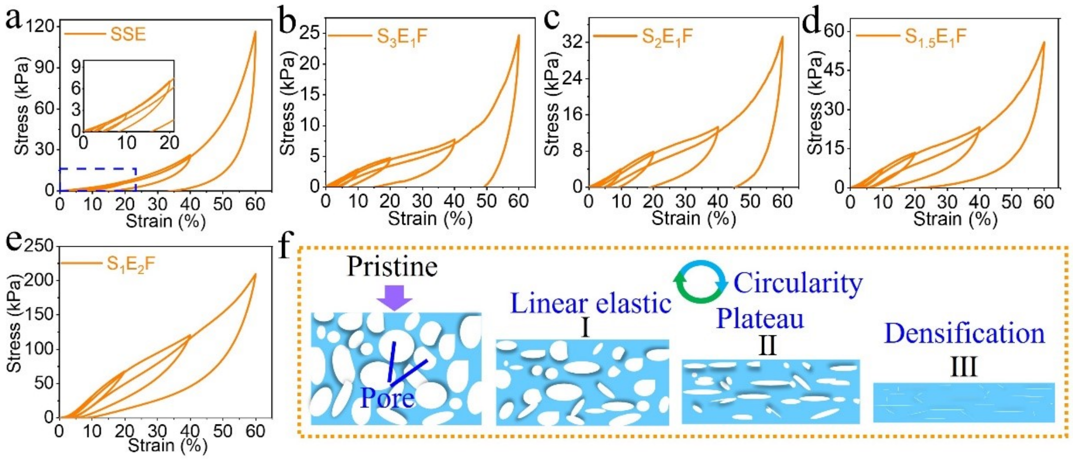

Fig. S3 Stress-strain curves of (a) SSE, (b) S_3E_1F, (c) S_2E_1F, (d) $S_{1.5}$ E_1F and (e) S_1E_2F with compressive strain increasing from 5% to 60% at 0.005 s^{-1} strain rate. (f) Compression mechanism diagram of SEF.

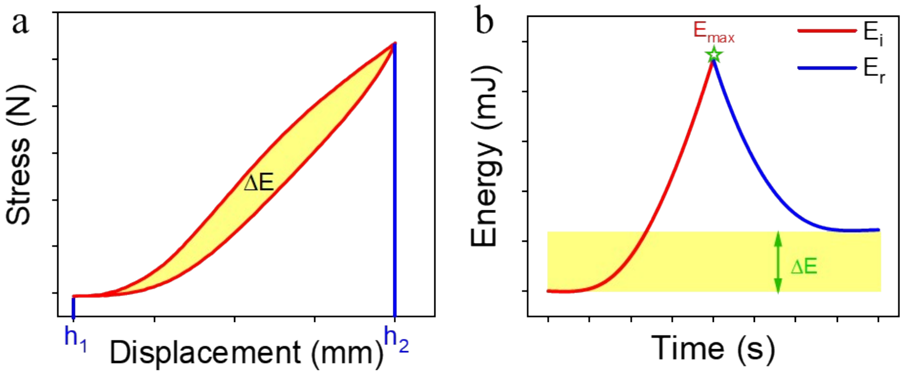

Fig. S4 The schematic of (a) energy loss and (b) energy loss coefficient of SEF.

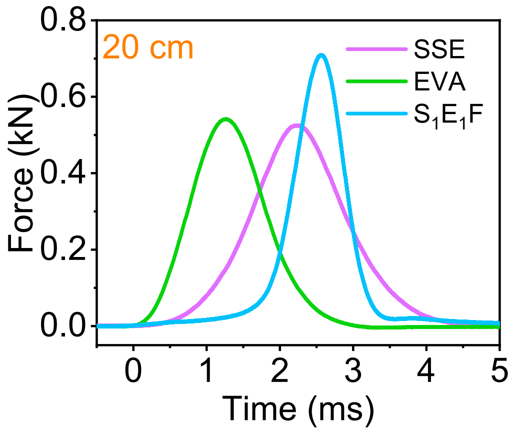

Fig. S5 Force attenuation of different composites at an impact height of 20 cm.

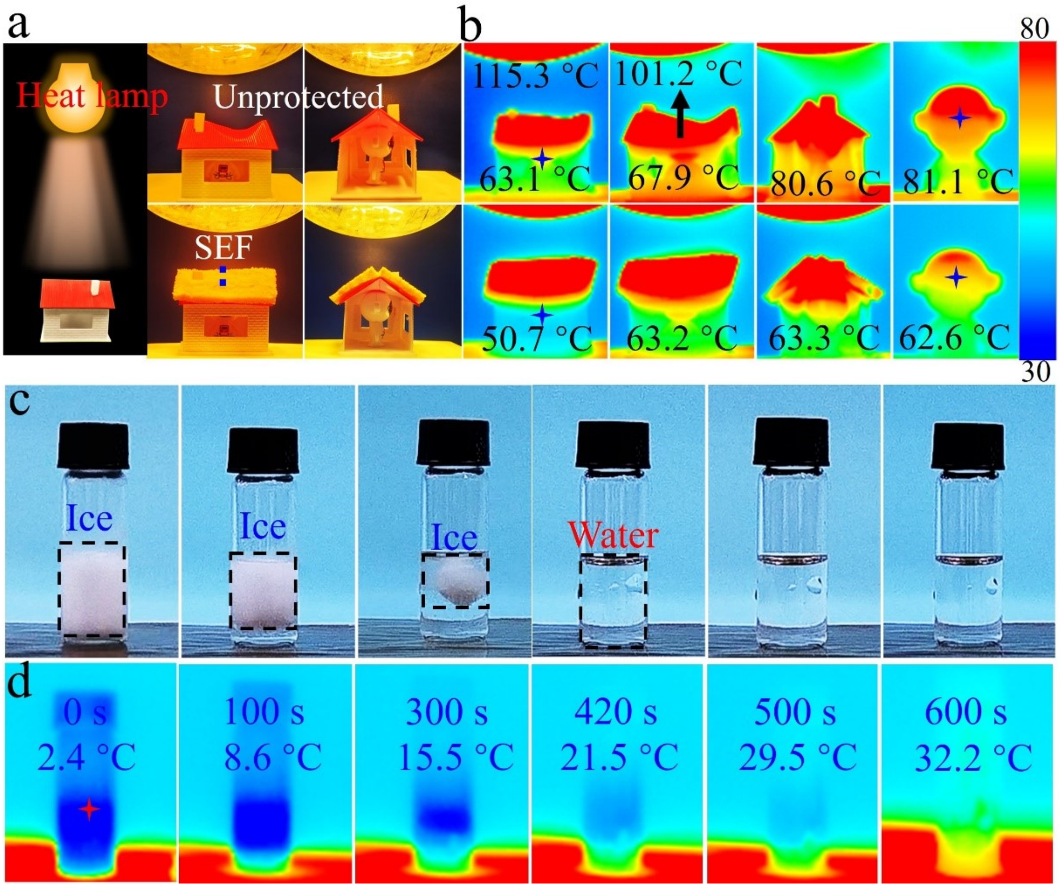

Fig. S6 The (a) schematic diagram and (b) corresponding infrared images of the model unprotected and protected with SEF in a high temperature environment. (c) Digital and (d) infrared images of the ice during melting.

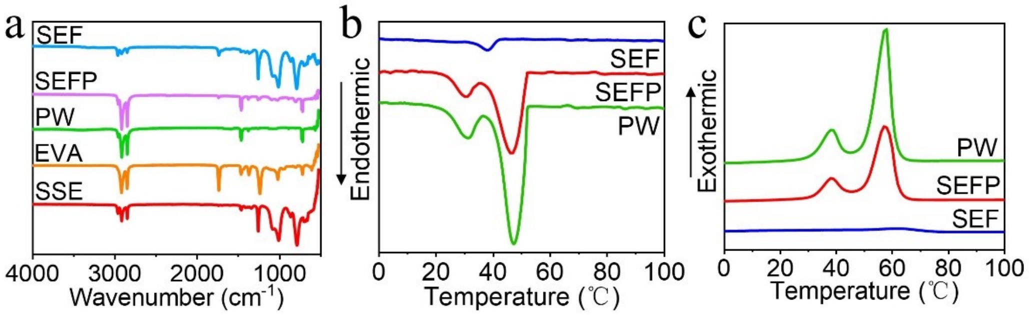

Fig. S7 (a) FTIR spectra of SEF, SEFP, PW, EVA and SSE. DSC curves of PW, SEFP and SEF during (b) crystallization and (c) melting.

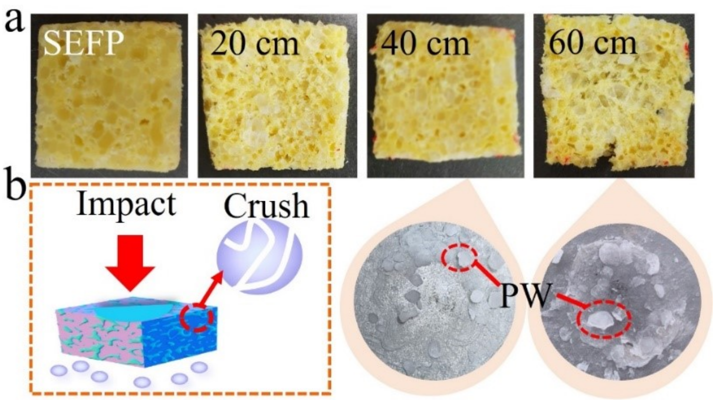

Fig. S8 (a) Surface topography and damage of SEFP under hammer impact at different falling heights. (b) Schematic diagram of protection mechanism of SEFP.

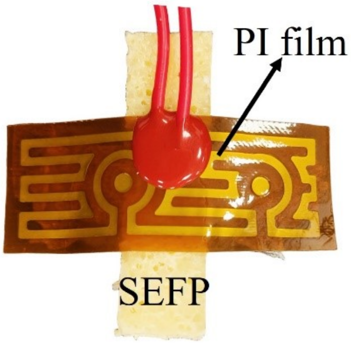

Fig. S9 Digital image of SEFP in fire suit at high temperature.

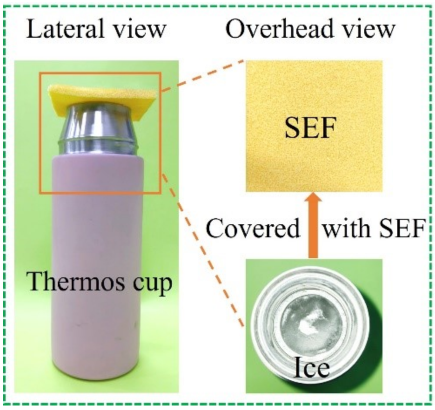

Fig. S10 Diagram of SEF using for thermal camouflage of low-temperature object.

Movie S1 Free fall protection experiment of beaker.

The morphologic change of the beaker free falling from 130 cm to different materials.

1 H. Qin, Y. Zhang, J. Jiang, L. Wang, M. Song, R. Bi, P. Zhu, F. Jiang, *Adv. Funct. Mater.*, 2021, **31**, 2106269.

2 H. Gao, Z. Wang, C. Cui, J. Bao, Y. Zhu, J. Xia, S. Wen, H. Wu, S. Yu, *Adv. Mater.*, 2021, **33**, 2102724.